VIRGO Purple Book

Version 2.1

May 1995

Documentation change record log 4
1 Introduction 6
2 Science Objectives 6
2.1 Helioseismology 14
2.1.1 Core structure 14
2.1.2 Radial stratification 14
2.1.3 Deviation from spherical symmetry 14
2.1.3.1 Internal rotation 15
2.1.3.2 Core magnetic field 15
2.1.3.3 Residual internal asphericity 15
2.1.4 g modes and convection 16
2.1.5 Excitation and damping 16
2.2 Radiometry 16
2.2.1 Solar energy budget and variability 18
2.2.2 Surface temperature variations 18
2.2.3 Active region flux budget 19
2.2.4 Diameter variations 19
2.2.5 Solar noise 19
3 Specifications and Requirements on Instruments and Subsystems 20
3.1 SPM 20
3.1.1 Wavelengths and Bandwidths 20
3.1.2 Detectors 21
3.1.3 Filters 21
3.1.4 Noise Levels 21
3.1.5 Observing sequence 22
3.2 LOI 23
3.2.1 Wavelengths and bandpasses 23
3.2.2 Optical System and Detector 23
3.2.3 Guiding System and diameter measurements 25
3.2.4 Noise levels 25
3.2.4 Observing sequence 25
3.3 PMO6-V 26
3.4 DIARAD 26
3.5 Data Acquisition System (DAS) 27
3.5.1 DAS Functional Description 27
4 Requirements and Specifications on Data Reduction Methods and Software 29

4.1 EGSE 29
4.2 Scientific processing 30
4.2.1 Primary Reduction 30
4.2.2 Instrumental and orbital effects correction 31
4.2.3 Secondary Reduction 33
4.2.3.1 Estimation of p-mode parameters 33
4.2.3.2 Determination of g-mode parameters 34
5 Theory developments hoped for 37
5.1 g-mode amplitude 37
5.2 Intensity "eigenfunction"and visibility 37
5.3 Excitation 38
5.4 g modes and convection 39
6 Interfacing with other Experiments 40
6.1 GOLF 40
6.2 MDI 40
6.3 SOHO Corona experiments 40
6.4 Ground Based experiments 41
7 References 43

Documentation change record log

ISSUE / REV.	SECTION / PAGE	DATE	CHANGES
1.0	All	7 Nov 94	N/A
1.1	All	6 Dec 94	Change Blue to Purple
	2	23 Nov 94	Add Scientific Obj. the *Sol.Phys.* article
	2.1	8 Feb 95	Tuning after C.Fröhlich's input
	2.1.5	25 Nov 94	Add input of T.Toutain
	2.2-2.2.3	7 Jan 95	After input from J.Pap
	2.2.4	26 Nov 94	Add Diameter Variations
	2.2	8 Feb 95	Tuning after C.Fröhlich's input
	All sections	23 Nov 94	Change name of PM06 to PMO6-V
	3	23 Nov 94	Add input of J.Romero
	3.1	5 Jan 94	Add data from the *Sol. Phys.* article
	3.1	31 Jan 95	Add inputs from Wehrli
	3.1.1	19 Dec 94	Add SPM filter profiles info. (ftp server)
	3.1.5	31 Jan 95	Add Fig SPM-I
	3.2	5 Dec 94	Add LOI detector configuration
	3.2.1	13 Dec 94	Add LOI filter profile information (ftp server)
	3.2.3	7 Dec 94	Add guiding results from Tenerife
	3.3	6 Jan 95	Add lifetime variation
	3.4	6 Jan 95	Add data from the *Sol. Phys.* article
	3.5	2 Feb 95	Add Roth's input
	4	24 Nov 94	Add EGSE Input from A.Jimenez
	4.2.1	24 Nov 94	Add Primary reduction input from A.Jimenez
	4.2.2	30 Jan 95	Add instrumental and orbital corrections

ISSUE / REV.	SECTION / PAGE	DATE	CHANGES
	4.2.2	3 Feb 95	Add guiding pixels' algorithm
	4.2.3	16 Nov 94	*p*-mode identification method
	4.2.3	25 Nov 94	Add *g*-mode identification technique and Lifetime information from B.Andersen
	4.2.3	27 Jan 95	Add noise simulation
	4.2.3	8 Feb 95	Re-ordering after C.Fröhlich's input
	5	23 Jan 95	Add Nice inputs
	5.2	9 Feb 95	Add Table 1 from Nice
	5.3	27 Jan 95	Add B.Andersen's input
	5.4	27 Jan 95	Add par. on *g*-mode transmission
	6.1	8 Feb 95	Add C.Fröhlich's input
	6.2	7 Jan 95	Add the data needed for the flux budget
	6.2	8 Feb 95	Tuning after C.Fröhlich's input
	6.3	5 Jan 95	Add B.Andersen's input
	8	23 Jan 95	Add References
2.1	Intro	21 Apr 95	Change VBB to VPB
	4.2.2	9 May 95	Remove spurious square root in (3)
	4.2.2	9 May 95	Change P_i for S_i for compatibility in (8)
	5.2	21 Apr 95	Change degree to order in Table 1

1 Introduction

The overall goal of this VIRGO Purple Book (VPB) is to ensure the best possible scientific output from the VIRGO investigation. To achieve this goal the VPB document will list and update the specifications and requirements of the different parts of the investigation, from objectives of the team members.

In the course of the development of the investigation it is hoped that this document will , at any given snapshot in time, give a status of how the scientific side of the investigation is developing. By using this document we should be able to pin-point the areas where we need to concentrate our efforts; the different team members will contribute where they see their efforts are needed. Some pushing from the PI and/or ES may be attempted.

This document will certainly go through a large number of revisions, in order to keep an ordered track on the development and the status of the latest Revision, the responsibility of updating the VBB is upon the VIRGO Experiment Scientist. Currently the VBB has a formal status within the VIRGO investigation and is under configuration control.

I would like also to take this opportunity to point out the successful detection of the *p* modes by the Tenerife LOI. The LOI has now been working for more than 9 months. A considerable advance has been obtained for checking the integrity of the instrument, its potential problem (none found so far), the mode isolation by the optimal filters, and the extraction of the information contained in the *p* modes. A letter to A&A was written for summarizing the findings (Appourchaux et al, 1995).

2 Science Objectives

The VIRGO experiment will provide the following observational and derived data:

- continuous high-precision, high-stability and high-accuracy measurements of the solar total and spectral irradiance and spectral radiance variation;
- continuous measurements of the solar polar and equatorial diameters;
- frequencies, amplitudes and phases of oscillation modes in the frequency range of 1 μHz to 8 mHz;

The total irradiance is measured with active cavity radiometers (PM06-V and the Dual Irradiance Absolute Radiometer, DIARAD), the spectral irradiance by three-channel Sunphotometers (SPM) and the radiance with 12 resolution elements on the solar disk using the Luminosity Oscillations Imager (LOI).

These data will be utilized to achieve the main scientific objectives of VIRGO summarized in the following list:

- detect and classify low-degree *g* modes of solar oscillations;
- determine the sound speed, density stratification and rotation in the solar interior, specifically determine the physical and dynamical properties of the solar core;
- study the solar atmosphere through comparison of amplitudes and phases of the *p* modes with these from GOLF (Global Oscillations at Low Frequencies) and SOI/MDI (Solar Oscillation Investigation/Michelson Doppler Imager);
- search for the long periodicities or quasiperiodicities that have been found in other solar parameters;
- utilize the solar `noise' signal to develop models for the global signature of stellar surface parameters;
- determine properties of the solar asphericity and its variation in time;
- study the relation between *p*-mode frequency changes and irradiance variations;
- study the influence of solar active regions and other large-scale structures on total and spectral irradiance;
- study the solar energy budget;
- provide accurate total and spectral irradiance data for input in terrestrial climate modelling.

Observations of the total solar irradiance will be a continuation of previous measurements from satellites, which have been performed by the radiometer HF of the Earth Radiation Budget experiment (ERB) on the NIMBUS-7 satellite from November 1978 until January 1993 (Hoyt et al 1992), by ACRIM~I on the Solar Maximum Mission satellite (SMM) from February 14, 1980 until June 1, 1989 (e.g. Willson and Hudson 1991), by ACRIM~II on the Upper Atmospheric Research Satellite (UARS) since October 1991 (Willson 1992) and by SOVA (Solar Variability) on the European Retrievable Carrier (EURECA) from August 1992 until May 1993 (Crommelynck et al 1993, Romero et al 1994).

The spectral irradiance data will resemble the data from IPHIR (Interplanetary Helioseismology with irradiance observations) on the Soviet PHOBOS Mission (Fröhlich et al 1990). As a secondary output the internal guider of the LOI component will produce time series of data proportional to the polar and equatorial solar diameters. All the data will have higher precision than any of those acquired formerly, both because of improvements to the instrumentation and because of the ideal location of the SOHO spacecraft which allows uninterrupted observation of the Sun. In addition, the spatial resolution of the LOI will allow us to deconvolve effects of different photospheric spatial variation on the solar irradiance, thereby enabling us to identify degrees and azimuthal orders of low-degree solar oscillations. The variations seen in these time series are a superposition of random and periodic phenomena that cause the whole variability of solar irradiance, both bolometric and at different wavelengths. This will be supplemented by even more detailed information from the flux budget product (128×128 pixels temporally averaged image of the solar disk), which will be studied in conjunction with the magnetograms provided by SOI/MDI on SOHO.

The scientific content of the gathered time series of irradiance can be studied in different ways. One way is to use it to observe and characterize solar oscillations. For the *p* modes the method has proven its value (e.g. Toutain and Fröhlich, 1992), and VIRGO will contribute by improving the reliability of the data to help resolve still controversial issues such as, for example, the temporal amplitude variation which is crucial for understanding in detail the excitation and damping mechanisms. But more important is the determination of the structure of the energy generating core. Of greatest interest, perhaps, is its relevance to the solar neutrino problem, for that has implications in other branches of physics. We do not even know for sure whether the neutrino problem is an issue in stellar-structure theory or is an issue in nuclear or particle physics. If it is the former, our task must surely be to investigate the wider implications in astrophysics. If it is the latter, it behoves us to determine the structure of the core - its radial stratification and its horizontal and temporal variations - as accurately as possible, in order to provide the most reliable information about the neutrino source to couple with the next generation of neutrino observations. To this end we need not only to model the variation of temperature, pressure and density, but also to try to model the related variation of chemical composition, both helium (hydrogen) abundance and the heavy-element abundances, using the direct seismic inferences. Together, the instruments on VIRGO will be able to provide extremely accurate frequencies of low-degree modes which are an essential complement to the intermediate- and high-degree data from SOI/MDI required to render it possible to carry out inversions for both the spherical and aspherical components of the stratification in the region where the thermonuclear reactions are taking place (Gough and Kosovichev, 1993).

The unambiguous detection and identification of solar gravity modes would be a real breakthrough for improving quite substantially our knowledge of the structure of the solar core. All attempts up to now have somehow failed because the amplitudes of the modes seem to be so small that the *g*-mode signals are buried in the noise (Fröhlich and Delache 1984). Although most of this noise is of solar origin, some observational and methodological improvements can be expected. Oscillation periods of several hours are difficult to observe from the ground and from satellites in low-Earth orbits; moreover, this range could not be explored by IPHIR owing to the noise introduced by the influence of the variability of the spacecraft pointing. This period range, however, looks promising for the search of *g* modes, because the modes are not as crowded in frequency as they are at lower frequencies, and the separation of the different l and m is easier. Nevertheless, the amplitudes may still be smaller than the solar noise. Probably, the only possibility to overcome this problem is similar to the heterodyne detection of a signal at a known frequency buried in noise. Another possibility may be to utilize the difference in centre-to-limb variation of the *g*-mode signal and the solar noise. The crucial point in the detectability of solar *g* modes is the surface amplitude of the modes. This again depends on the mode amplitudes below the convection zone and the amount of attenuation of the modes through the evanescent convection zone. Numerical modelling indicates that convective overshoot into the interior may excite the waves (Andersen 1994) to amplitudes that should be detectable at the surface. This result, however, may be uncertain due to the inadequate treatment of radiative damping in the interior.

We do not know the values of the frequencies of the individual modes, but we do have information from theory about the frequency pattern for different solar models, and the splitting as a functional of rotation (e.g. Berthomieu et al 1978, Provost and Berthomieu 1986) and asphericity. As several trials of this method have shown -- although with less reliable data and at lower frequencies --this *a priori* information alone may not be sufficient (e.g. Fröhlich and Delache, 1984). As a further ingredient the predicted relative visibility of different modes observed as intensity fluctuations and as Doppler shifts can be used. The relation between the different apparent amplitudes varies with frequency and depends also on the degree of the *g* mode (Berthomieu and Provost 1990), and thus the detection and unique identification of these modes may be possible only by combining data from VIRGO, GOLF and SOI/MDI, which are all on SOHO observing the Sun simultaneously. A reliable calculation of the visibilities is not available, however, because it must certainly be influenced by convection, which cannot reliably be modelled. It is important to realize that even if *g* modes cannot be detected the accurate measurement of low-degree *p* modes of low order, which VIRGO is well suited to accomplish, will augment quite substantially our diagnostic capabilities for investigating the structure of the solar core.

Solar irradiance variability can be used to investigate many physical phenomena related to convection, the effects of magnetic fields, solar activity, etc. (e.g. Fröhlich 1994). We may be interested in the phenomena causing the variation, e.g. sunspots, or we may be mainly interested in the underlying physical causes for the existence of sunspots, e.g. dynamo theory, rotation and convection. The causes of irradiance changes are crucially important for the understanding of solar and stellar evolution. Irrespective of the cause, knowledge of the possible medium- and long-term variations of the solar irradiance are equally important for the understanding of terrestrial climatic change. While the solar energy in the entire spectrum and particularly at UV wavelengths has been monitored from space for more than one and a half decades, no continuous space observations of the solar total and spectral irradiance has been made so far. Besides its climatic implications, knowledge of the amount of the solar energy flux and its variability at visible and red wavelengths is also important for solar physics. Comparison of visible and infrared solar radiation with surface manifestations of solar activity will give us a better understanding of the physical processes taking place in the photosphere. Parallel studies of the changes in the total flux and in various spectral bands will provide the first information on the spectral redistribution of the total flux variability.

These aperiodic or quasiperiodic phenomena are best studied in the time domain, where the variations may be compared directly with the signatures of solar surface intensity structures (e.g. Willson and Hudson 1988) or by multivariate spectral analysis (e.g. Fröhlich and Pap 1989). Although irradiance variations and solar oscillations are, for simplicity, currently treated independently, it is highly likely that these domains overlap physically. The influence of the changing magnetic fields during the solar cycle on the frequency of *p* modes and solar luminosity is one example (Kuhn and Libbrecht 1991, Bachmann and Brown, 1993). Moreover, the long-period solar oscillations may be coupled to the seemingly aperiodic or quasiperiodic variations in irradiance (which has been suggested, for example, by Wolff, 1984), either directly or by influencing surface intensity configurations. Although the solar background signal has the effect of a noise signal on the oscillation measurements, this 'noise' contains valuable information about the causative physical phenomena such as granulation, mesogranulation, supergranulation and active regions, which influence the dynamical oscillation frequencies. It will be necessary to take the modifications to the oscillation frequencies into account in order to establish what they would have been had the activity not been present, for it is those putative unmodified frequencies that are required for the structure inversions.

VIRGO SCIENCE RETURN (1)

Core structure	Mean values of pressure, density, temperature, chemical composition in the solar core region.
Radial stratification	Values for the spherically symmetric mean values of pressure, density, temperature, chemical composition as function of radius below the convection zone.
Internal rotation	Rotation as function of radius and latitude.
Core magnetic field	Investigate the possible existence of a strong core field.
Internal asphericity	Possible internal asphericity due to rotation or other effects.
g modes and convection	Study the interaction between *g*-modes and convection,quality of internal cavity and the upper boundary conditions, *g*-mode amplitude and phase coherence.
Core mixing	
Excitation and damping	Lifetime of *p* modes and possibly *g* modes (in combination with GOLF and SOI data), driving mechanisms.Visibility effects on the observability of modes. Frequency and splitting changes.

VIRGO SCIENCE RETURN (2)

Solar energy budget and variability	Spectral and total irradiance variation, spectral and spatial redistribution of energy, provide accurate input for terrestrial climate modelling
Luminosity changes and global effects	
Surface temperature variation	Structure and variability of large scale surface temperature inhomogeneities. Variation of *p*-mode amplitudes and visibility.
Active region flux budget	Active region influence on radiance and irradiance, study the possible energy storage in the convection zone
Diameter variations	Relative variation of equatorial and meridional diameter/limb darkening, possible surface asphericity.
Solar noise	Study global characteristics of small scale solar surface phenomena through study of the background non periodic signal.

2.1 Helioseismology

2.1.1 Core structure

In order to be able to determine the mean physical parameters in the vicinity of the solar core, i.e. density, temperature, pressure, chemical composition, it is necessary to detect and classify several low degree *g* modes. The frequencies of these *g* modes together with the *p*-mode information will through inversion techniques yield information on these parameters. With knowledge of the basic physical parameters one can determine whether the solar neutrino problem has solar or particle physics causes. Furthermore it will be possible to determine the degree of internal mixing during the solar evolution. This overall knowledge will be of crucial importance for the general understanding of stellar evolution.

2.1.2 Radial stratification

Since the structure of the solar interior is nearly spherically symmetric, it is meaningful to separate the radial stratification from any nonspherical effects. One of the goals of *p*- and *g*-mode seismology is the determination of the spherical averages of pressure, density, temperature, and chemical composition as a function of depth. Such a determination will strongly rely on a good description of the microphysics of the solar material, basically the equation of state and the opacity. Conversely, there are open questions in the equation of state and the opacity that will greatly profit from a solar diagnosis. Fortunately, there is a rough spatial separation of effects in the Sun. In the bulk of the convection zone opacity virtually does not play a role because the temperature gradient is essentially adiabatic. Beneath, the principal contributors to the equation of state (H and He) are nearly fully ionised, causing thus the opacity part of the heavier elements to be the principal physical issue.

Inversions of the sound speed from medium degree *p* modes indicate a sharp change near the bottom of the convection zone, the causes of which is not completely understood.

2.1.3 Deviation from spherical symmetry

The cause for the line splitting of *p* and *g* modes is the deviation from spherical symmetry. The largest effect is caused by the internal rotation curve. On top of this there is a possible modulation due to subsurface flows. An internal asphericity (caused by rotation/convection/*g* modes/gradients in μ/other dynamical instabilities?) may also introduce splitting. The same phenomena may also apply for *g* modes. In addition the presence of an intense magnetic field in the solar core will also generate *g*-mode splitting.

2.1.3.1 Internal rotation

The splitting of the different *g*-and *p* modes will depend on the internal rotation curve. Inversion techniques may yield the radial (from low degree modes) and latitude dependence (from medium degree modes) of the internal rotation. This knowledge is important to understand the solar evolution and thereby also the general stellar evolution. The interaction between rotation and convection (also *g* modes) may be important for the understanding of solar activity and the generation of surface emerging magnetic fields.

Current observational data indicate that the latitude dependant differential rotation persists throughout the convection zone and that the rotation is more rigid below the convection zone. The change in rotation curve may cause shears which can influence the oscillation modes.

From low degree *p*-mode analysis there are currently no indications that the core region is spinning extremely rapidly; the most probable values are one to at most four times the surface rotation rate. This is still controversial and only very low order, low degree *p* modes or *g* modes can resolve this issue convincingly.

2.1.3.2 Core magnetic field

The structure of the splitting of the *g* modes may yield information of the existence of a strong magnetic field in the solar core. This "frozen in" magnetic field may be the remnants of the field in the proto-Sun. It is not clear how it will be possible to disentangle the effects of the rotational and other asphericity splittings from the magnetic splitting especially if the field is aligned with the rotation axis.

2.1.3.3 Residual internal asphericity

Other deviations from spherical symmetry, probably much smaller than the above mentioned, may exist: i.e. caused by convection/mixing, solar cycle, large scale circulation, *g* modes, gradients in μ or other dynamical instabilities below the convection zone.

2.1.4 *g* modes and convection

The internal *g* modes are trapped in the cavity below the bottom of the convection zone. The amplitude variation as function of degree and order of the *g* modes will depend on the quality of this cavity and thereby the interaction between convection and *g* modes. The observed amplitudes of *g* modes will also depend upon the way they transverse the convection zone and on how they are manifested at the photosphere. These effects depend on frequency and will thus also indicate the effective depth of the convective zone at different horizontal scales.

2.1.5 Excitation and damping

It is now well agreed that *p* modes are excited by turbulent convection. The kappa-mechanism is rather efficient in the case of pulsating stars, but the amplitudes of the solar oscillations exclude this mechanism. Not only the dependence of the amplitude upon the frequency, but also the temporal modulation of solar *p* modes can be well described with a model of stochastic oscillator. The damping of *p* modes, however, depends on several effects: non-adiabatic interaction due to radiative transfer, coupling with the turbulent convection and scattering of the acoustic waves by turbulence. The first mechanism can explain the observed linewidths only above 4 mHz. The second one, between approximately, 2 and 4 mhz. The third mechanism seems to be the best candidate to explain the damping over the whole p-mode frequency range (1.5 to 6 mHz).

The lifetimes of modes is generally studied from the linewidths in the power spectrum. As the form of a line may be influenced by the way the time series are analyzed this method has yielded controversial results. The same may apply to the analysis of the amplitude modulation of modes. The truly continuous observations by SOHO and new method of time series analysis will possibly resolve this issue.

Studies have been carried out by the VIRGO team to determine the visibility, that is the surface amplitude of *g* modes in brightness and velocity. Together with investigations of the efficiency of the convection zone in exciting *g* modes these results will be the basis for the strategy to search for *g* modes.

2.2 Radiometry

Continuous observations of solar irradiance (both bolometric and at different spectral bands) from space within the last one and half decades led to the discovery of changes in the solar energy flux on time scales from minutes to the 11-year solar cycle (e.g. Hudson, 1988). The rapid irradiance fluctuations are related to solar oscillations (Woodard and Hudson, 1983; Fröhlich et al., 1990). The short-term irradiance changes from days to months are caused by active regions via the combined effect of dark sunspots and bright faculae (Willson et al., 1981). The most important discovery of irradiance observations is the enhancement of solar luminosity during the high activity part of the solar cycle (Willson and Hudson, 1988b) that has been attributed to the changing emission of faculae and the bright magnetic network (Foukal and Lean, 1988).

Since variations in the solar energy flux - persistent over long periods of time - may trigger climate changes, it is fundamental to understand the underlying physical mechanisms and thus the possibilities for a solar forcing of climate on time scales of decades to centuries. It has been assumed that the variations in the solar output are directly related to the magnetic field evolution over the solar cycle (e.g. Hudson, 1988; Kuhn, 1994; Harvey, 1994). However, sunspots, faculae and the magnetic network cannot account for all the observed variations in total solar irradiance. It has been shown that empirical models of total solar irradiance underestimate the observed changes at the maximum of both solar cycles 21 and 22 (Foukal and Lean, 1988; Pap et al., 1994). The current empirical models are developed with simple linear regression analysis that gives only an overall picture on the relation between solar irradiance and solar activity indices. Identification of the cause of the residual discrepancy is a difficult problem, since temporal changes in differential rotation in the interior of the Sun, a solar dynamo magnetic field near the base of the convective zone or large scale convective cells may all produce long-term changes in the solar luminosity (Kuhn et al., 1988).

The irradiance observations of the SOHO/VIRGO experiment and high resolution solar images, available from the ground and also from space by the SOHO/MDI instrument, will help to understand solar irradiance changes which are related to the effects near the surface. Parallel investigations of solar oscillations and variations in the solar energy flux provide additional information on the solar interior. Although solar irradiance variations and oscillations are studied separately, it is likely that these domains overlap physically. The long-period solar oscillations may be coupled to the non-periodic or quasi-periodic variations in irradiance, either directly or by influencing the causes of surface intensity configurations (Fröhlich, 1990). The ultimate goal is to understand (1) how, (2) why and (3) on what mechanism govern at different time scale the solar energy flux. From this reconstruction and prediction of the solar induced climate changes might be possible.

2.2.1 Solar energy budget and variability

Although it has been known for decades that the solar radiative output changes through the entire spectrum, being much higher at wavelengths below 200-300 nm (e.g. Lean, 1991), the spectral distribution of total irradiance variability is not known as yet. Since the Sun's energy input is the main driver of the physical processes within the Earth's atmosphere, understanding the underlying physical mechanisms and determining the contribution of various spectral bands to the total flux variability are at the center of studying the climate impact of solar variability. The VIRGO integrated-light and spectral irradiance observations in the near-UV, visible, and near-IR, together with the UV observations of the UARS, NOAA9, and NOAA11 satellites, will provide the first real opportunity to estimate the spectral distribution of the changes in the solar energy flux.

2.2.2 Surface temperature variations

Kuhn et al. (1988) and Kuhn and Libbrecht (1991) have reported the results of solar limb brightness observations that are capable of explaining the total irradiance variation over the solar cycle. The solar limb flux, observed as a function of latitude, has been divided into "faculae" and "temperature part" based on the assumption that the temperature part remains constant during the observations, whereas the faculae appear as intermittent bright features. The temperature signal consists of two parts: a high-latitude temperature drift (>50 degrees) part which is attributed to a temperature change caused by e.g. a meridional circulation, and a low latitude part, which reflects the "active" latitude zone and is obviously related to the solar cycle. The analysis by Kuhn et al. (1988) suggests that changes in this low latitude thermal flux are responsible for causing part of the irradiance variations which is not due to active region faculae. The weakness of this result is based on the fact that it depends strongly on the limb darkening function assumed to extrapolate the observation at the limb to the full disk. Further studies are required and direct comparison of the total irradiance observations with the flux budget data from MDI/SOI and broad-band ground-based photometry will improve our understanding substantially. Moreover, the studies may tell which part of the long-term irradiance variability is due to magnetic surface effects and which part due to truly global effects.

2.2.3 Active region flux budget

Large complex sunspot groups can cause dips in total solar irradiance as large as 0.3%, whereas the irradiance excess due to the bright faculae is about 0.08% (Chapman, 1987). An important question in this context is whether the missing energy in the sunspot-related irradiance dips is re-radiated in the surroundings or is just stored below the surface and slowly emitted over time periods much longer than the life time of the spots. This question will be directly addressed by comparing irradiance data from VIRGO with so called flux budget intensity images (128×128 pixels) and magnetogram provided by SOI/MDI.

2.2.4 Diameter variations

The LOI will be able to measure diameter variations with a precision of about 0.3" for a 1.5-hour integration time. The oblateness will be measured with a precision of 0.3" for a 1.5-hour integration time. The variations will be calibrated using the changing size of the Sun which is corresponds to a variation of +/-3% during the course of a year. The calibration will be performed with an accuracy of about 1% for a 6-month observation time. The estimate of the uncertainties comes from the LOI operated at Tenerife in 1994/95 and gives only an upper limit as the atmosphere perturbs the measurements in many ways. The data on solar radius can be combined with total irradiance data to yield the relation between them, the result of which is of crucial importance for the understanding of global changes of the Sun. This relation yields information about the depth of the perturbation.

2.2.5 Solar noise

The shape, time variation and amplitude of the solar noise signal is directly dependent of the flux parameters of solar surface structures. From the study of this signal it will be possible to deduce the global characteristics of granulation, mesogranulation, supergranulation and active regions. This information is necessary to enable the investigation of such structures on other stars.

3 Specifications and Requirements on Instruments and Subsystems

The contents of this chapter will describe the specific requirements on the VIRGO components and subsystems in order for the observables to meet the scientific objectives as described in chapter 2.

3.1 SPM

3.1.1 Wavelengths and Bandwidths

The choices of the SPM wavelengths are made partly of scientific, partly of technical reasons and partly out of prejudice. The scientific background is to get an observational handle on the spectral redistribution and variation of global oscillations and solar variability. The Si detectors are effectively limited to observe at the required accuracy between 320 and 900 nm. The original proposal had the shortest wavelength at 335 nm, but this was discarded because of the extreme sensitivity to contamination at this wavelength, this was shown with the IPHIR experiment. The 402nm wavelength was chosen as a short wavelength compromise and because it permits the use of more stable filter glasses and lies just above the Ca II H&K lines; going into the H or K lines would give a small advantage only with a high spectral resolution. The visible and near-infrared channel wavelengths are mainly due to the history of previous experiments.

Wavelengths:	402 nm
	500 nm
	862 nm
Bandwidths:	5 nm
	5 nm
	5 nm
Effective bandpass	The spectral profiles can be found on the ftp server:ftp.estec.esa.nl/pub/loitenerife/PurpleBook. They are ascii files called virgospmblu.dat, virgospmgrn.dat, virgospmred.dat with 2 columns (wavelength, transmission).
Effective opacity /optical depth:	To be derived from the bandpasses

3.1.2 Detectors

The detectors are silicon photodiode S1337 from Hamamatsu, Japan mounted in a common housing with the interference filters.

Power on detectors	402 nm:	23 μW
	500 nm:	28 μW
	862 nm:	30 μW
Lifetime sensitivity variation:	402 nm:	95% (IPHIR and SOVA2, 335 nm)
	500 nm:	49% (IPHIR and SOVA2)
	862 nm:	17% (IPHIR and SOVA2)
Detector stability		
Temperature sensitivity (effect of the filter included)		
	402 nm:	-710 ppm/K
	500 nm:	-1040 ppm/K
	862 nm:	-270 ppm/K
Aging		
	402 nm:	TBD
	500 nm:	TBD
	862 nm:	TBD

3.1.3 Filters

Filter degradation

Temperature sensitivity:	See above
Particle sensitivity:	
Transmission drop:	402 nm: 52%
	500 nm: 7%
	862 nm: 1%
UV sensitivity:	No UV data available (yet!)
Surface contamination:	Unknown
Angular sensitivity:	Unknown

3.1.4 Noise Levels

Amplifier and resistors:	included in total instrumental noise
V/F converters:	included in total instrumental noise

Total Instrumental Noise

Short Term (above 1 mHz)	402 nm:	See Fig SPM-I
	500 nm:	better than at 402 nm
	862 nm:	better than at 402 nm
Long Term (below 1mHz)	402 nm:	See Fig SPM-I
	500 nm:	better than at 402 nm
	865 nm:	better than at 402 nm

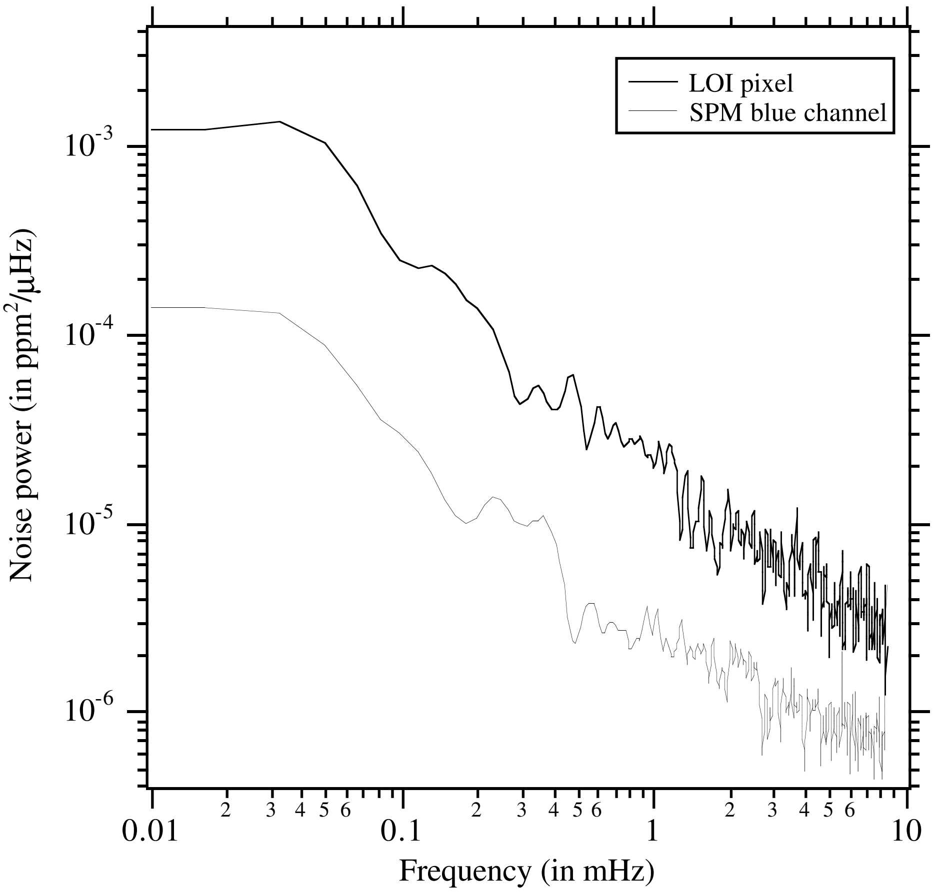

Figure SPM-I: Power spectral density of the dark-current noise of the SPM blue channel, and an LOI pixel calculated from time series of 68 h and 45 h respectively. In the 5-minute range the noise of the SPM is about 5×10^5 times smaller than the noise between the p modes of IPHIR (= 0.5 ppm^2 μHz^{-1}). For the LOI pixel it is about 1.2×10^6 times smaller than the noise expected for a 12th of the solar disk (12 time the noise power of the full disk)

3.1.5 Observing sequence

Please refer to the VIRGO operation manual.

3.2 LOI

3.2.1 Wavelengths and bandpasses

The LOI wavelength and bandpass is chosen to be the same as the 500 nm channel of the SPM. This allows the instruments to be calibrated to each other.

Filter:	500 nm
Bandwidth:	5 nm
Effective Bandpass:	The spectral profile can be found on the ftp server: ftp.estec.esa.nl/pub/loitenerife/PurpleBook. It is an ascii file called LOIAndover.dat with 2 columns (wavelength, transmission).
Effective opacity /optical depth:	To be derived from the bandpass

3.2.2 Optical System and Detector

Telescope: Ritchey-Chrétien with a 1300-mm focal length, diameter 55 mm, central obstruction 25 mm.

Detector: Deep diffused silicon photodiode with 12 scientific and 4 guiding pixels as given in Figure LOI-1. The crosstalk between pixel is smaller than 10^{-4}.

Power on detector: 0.8 mW/cm^2

Detector stability

Temperature sensitivity: about 50-100 ppm/K
Aging of temperature sensitivity: drift of -400 ppm/K to be controlled with a ground copy of the flight detector

Filter degradation

Temperature sensitivity: to be measured
UV sensitivity: No degradation after 1 year of solar UV (below 400 nm)
Particle sensitivity: 5% relative transmittance drop after a 7-year SOHO dose.
Surface contamination: temperature of the filter should be about 10 ^{0}C higher than the structure, and should prevent condensation of contaminants.
Angular sensitivity: Unknown

LOI Detector flight configuration
Scale 14:1

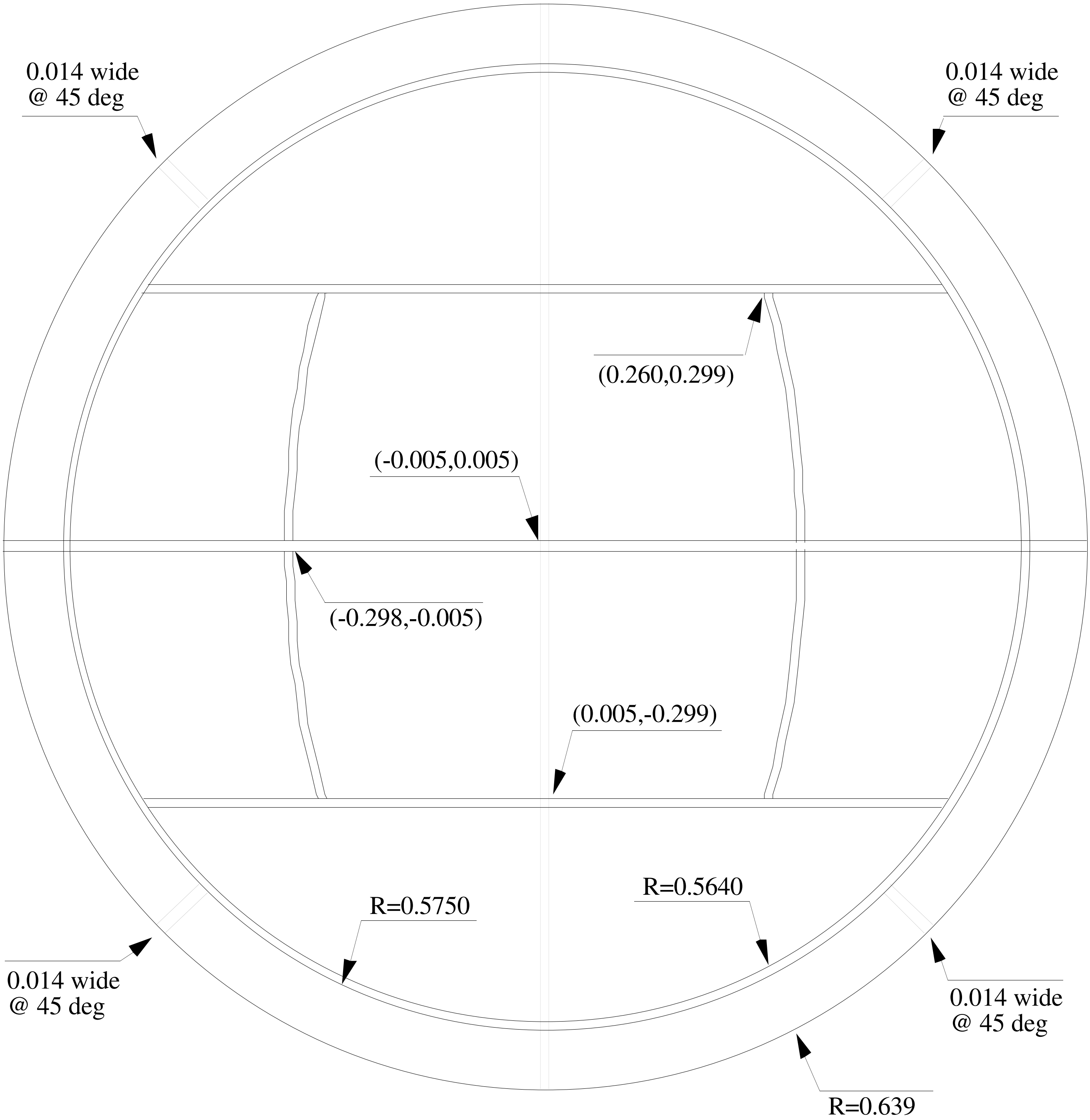

All dimensions are in cm
All tracks are 0.01 cm wide except where annotated
The detector is symmetrical about the centre
LOI focal length is 130.7 ± 0.079 cm (measured on 11 Octobre 1993)
The equation of the elliptical part of the detector are given by *a*=0.303 cm and *b*=0.613 cm
The ellipse is in the middle of the tracks
T.Appourchaux, 18 Octobre 1993

Figure LOI-1

3.2.3 Guiding System and diameter measurements

Guider stability and range: 0.1" and ± 8.5'

Thermal stability : 0.2'/K

Hysteresis: 10%

Voltage sensitivity: 16' for 650 Volts

Aging: unknown

High voltage supply: -150 to 450 Volts

Servo loop aging: unknown

Guiding power Spectrum:

EW axis: 5 "/√Hz @ 0 Hz, 3.2 "/√Hz @ 9000 μHz, linear dependence in the power spectrum, σ=0.4".

NS axis: 3.16 "/√Hz @ 0 Hz, 2.23 "/√Hz @ 9000 μHz, linear dependence in the power spectrum, σ=0.26"

Diameter Measurements: Spectrum rather flat 3.2 "/√Hz, σ=0.17".

The above power spectra are based on ground-based measurements. They are essentially limited by the atmospheric seeing and its associated transparency changes. These spectra should, hopefully, be better in space.

3.2.4 Noise levels

Electronics stability

VF converters: 1 ppm/K

Instrumental Noise

Short Term (5-min range): <0.5 ppm^2/μHz (ground-based measurements, limited by the atmosphere)

Dark current noise: See Fig SPM-I

Long Term: unknown. Most of the noise contribution will be due to the temperature fluctuations on the filter and detector.

3.2.4 Observing sequence

Please refer to the VIRGO Operation manual.

3.3 PMO6-V

Two fully characterized instruments (absolute instruments): the "active" instruments measuring continuously and a "back-up" instrument ensuring redundancy and monitoring of the degradation of the active instrument.

Cavity

Lifetime variation: 30 ppm/year

Absolute accuracy: 0.17%

Sampling rate: 1 solar total irradiance / 2 minutes

Duty cycle: 17%

Resolution: 50 ppm

Instrumental Noise

30 ppm (standard deviation of the "dark irradiance" every 2 minutes)

White noise, <0.4 $ppm^2/\mu Hz$

Temperature dependence: TBD

The following instrumental corrections will be needed:

- Temperature dependence of the electronics
- De-pointing
- Thermal exchanges with the environment
- Degradation of the sensor

Please refer to the VIRGO Operation manual for the observing sequence of the PMO6-V.

3.4 DIARAD

Cavity

Lifetime variation: 30 ppm/year

Absolute calibration: 0.15%

Sampling rate: 1 solar total irradiance / 3 minutes

Duty cycle: 11%

Instrumental Noise

White noise, <0.4 $ppm^2/\mu Hz$

The following instrumental corrections will be needed:

- Temperature dependence of the electronics

- De-pointing
- Thermal exchanges with the environment
- Degradation of the sensor

Please refer to the VIRGO Operation manual for the observing sequence of the PMO6-V.

3.5 Data Acquisition System (DAS)

3.5.1 DAS Functional Description

The Data Acquisition System (DAS) comprises the OBDH interface for telemetry, telecommands and timing signals. The controller is based on a hardware sequencer with a 2 Mbits memory for 25 hours autonomy of data storage. The scientific objectives of the VIRGO investigation relies on long and uninterrupted time series. These time series are analyzed by calculating power spectra, the noise of which depend strongly on the way the sampling is done. Ideally one should integrate the signal during the whole sampling interval; otherwise high frequency noise leaks into the power spectrum. As the integration time relative to the sampling interval decreases, the power of the folded-in high frequency noise increases. It has to be noted that this noise is an inherent part of the time series and can not be reduced by a posteriori filtering of the time series. Simulation experiments have shown that in the case of solar observations with a sampling corresponding to a Nyquist frequency around 10 mHz, integration during at least 90% of the sampling interval is needed to reduce the folded-in noise to tolerable levels. Technically, this is best achieved with parallel voltage-to-frequency converters (VFC) which allow for true integration over a given time interval.

The data acquisition is performed by parallel VFCs with a full scale frequency of about 320 kHz. The basic sampling period is 10 s allowing for a theoretical resolution of 0.3 ppm for one reading. Within the 10 s period the signals are integrated during 9.4 s whereas the rest of the period is used for the calibration of the VFC with reference signals (400 ms, fs-resolution: 16 bit) and the reading and resetting of the counters (twice 100 ms). This timing allows for a continuous electrical calibration and a high duty cycle of the reading (94%). The electrical calibrations are performed in turn at three points, namely zero, half full scale and full scale allowing for a first order correction of the non-linearity of the VFC during the evaluation of the data. With this system it is necessary to have as many parallel channels as signals to be measured simultaneously. 10 VFC are for the science data and 1 VFC for the HK channel.

To calibrate the VFCs and to supply internal and instrument thermistors, a set of two independent reference elements with amplifiers are implemented to supply reference voltages of 2.5V as half scale reference (HS), 3.5V as full scale reference voltage for the housekeeping channel (HK) and 4.04V for full scale reference for the science channels. This reference voltage, used for calibration of A/D channels, is indicated on "DAS Status" word on the data files HK or Sc.

4 Requirements and Specifications on Data Reduction Methods and Software

Explanation of the data chain. It is so far very unclear where to start and here any contribution is welcome.

4.1 EGSE

The Electrical Ground Support Equipment (EGSE) is conceived to support the electrical verification and operation of VIRGO during the development and verification phase at instrument and system level. The EGSE is interfaced either to the Spacecraft Interface Simulator (SIS) for stand-alone operation or to the Common Check-out Control (CCS) system during system test. Moreover, the EGSE is used at the Experiment Operations Facility (EOF) during the first phase of the mission: that is, during start-up of the experiment and commissioning. Because of the rather simple tasks to be performed by the EGSE, a 386 type PC running MS-DOS has been chosen. The software is written in MOdula-2 and has been developed according to the ESA Software Engineering Standards. The EGSE software package comprises four main programmes:

1) VIRGO EGSE Operation Software (VEOS). This Software allows direct commanding (when used with the SIS) and receiving (on-line) of telemetry and displays all the data on different selectable screens.

1.1) Hexadecimal Screens.
All real time telemetry received in hexadecimal format at byte level. One screen for Science and other for HK.

1.2) Unpacked screens.
All real time telemetry received in number of counts at variables level. One screen for Science and other for HK.

1.3) Instruments screens in engineering units following the requirements of instruments CoI's. Four screens, SPM, PMO, DIARAD, and LOI, in real time telemetry.

1.4) VIRGO Engineering screens.
- 1.4.1) VIRGO 1: Temperatures and general status screen.
- 1.4.2) VIRGO 2: Current consumption ,voltages and HK calibration screen.
- 1.4.3) VIRGO 3: Analog channels (1 to 4) screen (DIARAD).
- 1.4.4) VIRGO 4: Analog channels (5 to 10) screen (SPM,PMO,Back-Up).
- 1.4.5) VIRGO 5: Digital channel (LOI) screen.
- 1.4.6) VIRGO 6: Analog channels calibrations screen.
- 1.4.7) VIRGO 7: VIRGO status screen.

Other facilities of VEOS is the execution of tests (when used with SIS), copy the received telemetry to a floppy disk.

2) Virgo EGSE Block Reader (VEBOR). The VEBOR programs performs the same function as the VEOS program but in off-line situation reading the data files archived by VEOS. It permits to see the same data screens, block by block. It also permits to the user to obtain 6 summary instruments files and compare the real time blocks with the corresponding -12h and -25 h blocks in order to know if some of them is missing or wrong.

3) Virgo Egse Packages Reader (VEPAR). This program only shows the data (off-line) at level acquisition mode. That is, raw data in hexadecimal format. As opposed to the VEBOR program it shows the information package by package as they have been received. Hence, this is the only way the user may check in detail the information received, because with this program it is possible to read all stored data, even idle packets, etc.

4) Virgo Egse COnstants Definitions (VECOD). It allows to modify some constants used by the program to make calibrations. This constants are different depending on the VIRGO model. So, there exist four groups of constants stored in different files: Proto-Engineering model (VEOS.PEM), Engineering model (VEOS.EM), Proto-flight model (VEOS.PFM) and Flight model (VEOS.FM). With this program the user can change and stored for further sessions the values of the constants.

More information about the EGSE utilities are in the EGSE User Manual (VIR-IAC-GSE/-003).

4.2 Scientific processing

4.2.1 Primary Reduction

VIRGO telemetry comes by packets , 3 for scientific and 4 for HK. One scientific block is built with the corresponding 3 Science packets and one HK block with the corresponding 4 packets. Idles packets are in between and also the different retransmittions (-12h. and -25h.). The first step to be done is to isolate the real time blocks from idles and retransmitted ones to built a consistent interrupted time series of real time telemetry blocks

A total number of 480 blocks per day are expected. The aim of this first step is to get those 480 blocks per mission day. If some of them are wrong or missing in real time telemetry , the delayed telemetry will be used to replace them in the blocks time series. In the worst case that even retransmitted blocks are missing it would be necessary to wait to CD rom disk to have the last opportunity two get the data, if they are still missing those data are lost and zeros will be input in their places with the corresponding mission day and block of day in the headers.

Once the real definitive blocks series are obtained, the instrument files (at number of counts levels) will be generated for each instrument, obtaining complete time series for each instrument (SPM,PMO,DIARAD,LOI, engineering) with all the required information (Science and HK) necessary (TBC) for the analysis as requested by instrument CoI's.

After this level 0, the level 1 will be produced following the calibrations algorithms and known corrections supplied by instruments CoI's. During normal operation VDC will check for aberrant values in the Science or HK data, signalling when corrective actions needs to be taken.

4.2.2 Instrumental and orbital effects correction

SPM

The solar spectral irradiance $S_{\lambda 0}$ at 1 astronomical unit (1AU) is given by:

$$S_{\lambda 0} = S_{\lambda m} \frac{r^2}{\cos\theta} \frac{1-\left(\frac{V}{c}\right)^2}{(1+\frac{v}{c})^2} \tag{1}$$

where $S_{\lambda m}$ is the measured spectral irradiance at the L1 point, r is the distance of the satellite to the center of the Sun, V is the satellite velocity in the frame linked to the Sun, v is the satellite velocity along the line of sight (v=V cos α), c is the speed of light (the correction due to V is of the order of 10^{-2} ppm)., θ is the off-axis angle between the line of sight and the optical axis of the LOI instrument; r is given by:

$$r = \sqrt{x^2+y^2+z^2} \tag{2}$$

where x, y and z are the heliocentric coordinates of the satellite; v is given by:

$$v = \frac{1}{r}\left(x\,\frac{\mathrm{d}x}{\mathrm{d}t} + y\,\frac{\mathrm{d}y}{\mathrm{d}t} + z\,\frac{\mathrm{d}z}{\mathrm{d}t}\right) \tag{3}$$

V is given by:

$$V = \sqrt{\left(\frac{\mathrm{d}x}{\mathrm{d}t}\right)^2 + \left(\frac{\mathrm{d}y}{\mathrm{d}t}\right)^2 + \left(\frac{\mathrm{d}z}{\mathrm{d}t}\right)^2} \tag{4}$$

And finally, the angle θ in rad can be derived from the high voltage on the Y and Z axis of the LOI instrument:

$$\theta = 0.000291 \sqrt{\theta_Z^2+\theta_Y^2} \tag{5}$$

with

$$\theta_Z = a\,HZ + b\,HY - c \tag{6}$$

$$\theta_Y = b\,HZ + a\,HY - c \tag{7}$$

where HZ and HY are the high voltage on the actuators of the LOI, a, b and c are calibration factors (FM, a=0.031 '/Volt, b=-0.00367 '/Volt, c=3.56'; FS, a=0.030 '/Volt, b=-0.0017 '/Volt, c=3.7')

LOI

The current on each scientific pixel has to be corrected from 3 main effects:

- Correction of distance
- Correction of line-of-sight velocity
- Temperature effect on detector.

The first effect is to the first-order negligible; this is due to the combined effect of an increased flux with a bigger Sun (the net variations is zero). To the second order, there will be a contribution from the limb darkening; this effect has yet to be computed. The second effect is a relativist contribution. The last effect is due the temperature sensitivity of the quantum efficiency of the silicon detector. The net correction can be written as:

$$S_i\,(1\,AU) = S_i\ \frac{(1+T\,q_T\,)}{\cos\theta}\,\frac{1-\left(\frac{V}{c}\right)^2}{(1+\frac{v}{c})^2} \tag{8}$$

where S_i is the current on scientific pixel i , T is the mean temperature, in ^{o}C, of the detector as measured by the 4 temperature diodes, q_T is the temperature dependence at 0 ^{o}C.

For the guiding pixel, the same remarks apply except that the changing size of the Sun should be taken into account in the first effect. And we write for the 4 guiding pixels:

$$G_j\,(1\,AU) = G_j\;\frac{(1+T\,q_T^G\,)}{\cos\theta}\;\frac{1-\left(\frac{V}{c}\right)^2}{(1+\frac{v}{c})^2}\left(\frac{r^2 - R_{sun}^2}{1 - R_{sun}^2}\right) \tag{9}$$

where q_T^G is s the temperature dependence at 0 °C for the guiding pixels. The last term is the effect of the changing size of the Sun, where R_{sun} is the size of the Sun with respect to the inner radius of the guiding pixel (=1.0556 after Figure LOI-1). This latter number will be refined and calibrated during the mission.

The full effects due to the limb darkening will be implemented in due time.

PMO6-V

The total solar irradiance S_0 at 1 astronomical unit (1AU) is given by:

$$S_0 = S_m\;\frac{r^2}{\cos\theta}\,\frac{1-\left(\frac{V}{c}\right)^2}{(1+\frac{v}{c})^2}\,(1+c_t t\,) \tag{10}$$

where S_m is the measured total solar irradiance at the L1 point, c_t is the rate of change of the relative difference between the measured irradiances between the nominal instrument and the back-up one.

In addition, a thermal model taking into account the radiative exchanges of the cavity with its environment must be developed for the PMO6-V radiometers. It will include the exchanges with the muffler during the open and closed states as well as the losses of the cavity to space in the open state.

DIARAD

Same as PMO6-V

4.2.3 Secondary Reduction

4.2.3.1 Estimation of *p*-mode parameters

More than one team should reduce the data for cross-checking each other. Even doing the same processing on two different machines taught us a lot with the data from the LOI in Tenerife.

The maximum likelihood method (MLE) give still the most reliable estimates of the *p*-mode parameters. When working with the data of the Tenerife LOI, we found that fitting simultaneously the $2l+1$ spectra of a given l gave the less noisy estimates of the frequency and the splitting. One of the main advantage was to have a common linewidth for the $2l+1$ components (Appourchaux et al, 1995).

The mode identification of *p* modes has been tested with the data of the Tenerife LOI and is based on the fact that for modes that stand out clearly out of the noise this is easy. The others are identified with a table of frequency (S/N<3) and their existence is checked statistically using MLE and a modified R-test. Modes, which have never been identified before, will be looked for using theoretical frequencies and the MLE.

The lifetimes of the individual *p* modes may be studied indirectly or directly with three different methods:

1) The linewidths of the time-averaged peaks in the power spectrum is among other effects directly related to the excitation and decay time of the individual modes occuring in the time span of the observations. This method is most applicable for the statistical analysis of many modes and the linewidths (lifetime) variation as function of frequency and/or *l* and *n* values.
2) A long time series may be divided into a sequence of overlapping shorter time series, eg. 30-day intervals shifted sequentially by one day. These spectra can be looked at by comparing the individual modes to a constant sine wave of the frequency of the mode and determining its phase and amplitude with a bi-variate spectral analysis. From the temporal variation of the phase and amplitude the excitation and damping of individual modes can then be extracted.
3) Wavelet methods, as opposed to Fourier methods, do not assume a stationary signal. Experiments have been made that indicate the usefulness of these methods to study the detailed time variation of the modes. The results are compatible with the ones using method 2), but has somewhat higher time resolution for a given dataset (about 25%). These methods may be used to study in detail differences in excitation of individual m components of a mode set.

4.2.3.2 Determination of *g*-mode parameters

Mode identification methods, g modes

The achievement of the main scientific goals of VIRGO depends on the identification and classification of solar global *p* modes. Since no unambiguous measurements of these modes have been made there is no definite estimate of the amplitudes. The basic assumption of the VIRGO team is that in the region from 30-120 μHz the signal will be dominated by the influence from solar "noise" and that the *g* modes will not be distinguished easily. Simulations of the solar "noise" have been carried out

(Andersen et al, 1994). These simulations indicate that in this range, the solar signal is comparable with the observations of ACRIM-SMM and is thus well explained by super-, meso- and granulation. The instrumental noise level of the VIRGO observations should be lower than this solar "noise" by at least the same factor.

The main strategies to look into the "noise" are the following:

1. Cross-correlation methods as described by Fröhlich and Delache (1984). These methods assume apriori knowledge of the *g*-mode frequencies and that they occur in a known pattern. This method is forceful if the current understanding of interaction between physical and dynamical parameters in the solar interior is reasonably correct. Assuming this it will be possible to generate a set of multidimensional arrays in the parameter space (internal rotation curve, properties of internal cavity ++) and find the best cross-correlation with the observed data. If the theory is correct, it should be possible to detect indications of *g* modes with power peaks which 5-10 times smaller than the solar noise. At 50 μHz this would give (with the power spectrum of ACRIM of 180 $ppm^2/\mu Hz$, for a 6-month observation and a S/N ratio of 0.1), a lower limit of 3 ppm on the amplitude of the detectable *g* modes. The main problem with this method is that it requires that the theory closely describes the solar interior.

2. The Center-to-Limb Variation (CLV) of the *g* modes in radiance depend on the combination of the induced variation in temperature/opacity and geometric deformation caused by the oscillation. This CLV should be different than that of the sources of the solar noise. This opens the possibility of reducing the effects of the noise on the oscillations observation by spatial and temporal filtering. This method has not yet been developed.

3. The signatures of *g* modes and solar noise are different for velocity and brightness measurements. This opens a further possibility to distinguish between noise and *g*-mode signal by combining data from VIRGO, GOLF and MDI. First results of a theoretical investigation of the visibility differences has been undertaken; a study for the possible noise suppression has not yet been attempted.

4. Methods have been developed assuming statistical knowledge of the noise signal (Andersen and Domingo, 1988, Germain (submitted to SP)) to suppress the noise. For the *p*-mode region and atmospheric sources for noise these methods have had some success. The efficiency of these methods in the *g*-mode frequency region are more difficult as a detailed knowledge of the solar noise source is not available. Again, data from MDI might help to get a better definition in this frequency range.

5. Wavelet analysis is a powerful tool to study impulse functions. The basic assumption concerning global solar g modes is that they have lifetimes longer than the SOHO mission duration. In this context no extra information will be obtained concerning p modes using wavelet analysis. However, the wavelet method may enable us to describe the properties of the solar noise signal such that it may be possible to reduce its influence on the g-mode signal.

5 Theory developments hoped for

5.1 *g*-mode amplitude

The *g* modes are trapped in the inner solar radiative zone and except for the very low degree modes their amplitude at the surface is very small relatively to its value below the convection zone. No theoretical estimation of the amplitude is actually available. For the computation of the predicted brightness variations due to *g* modes we need to give some values to the surface amplitude. One possibility is to assume arbitrarily equipartition of energy between the modes.

5.2 Intensity "eigenfunction"and visibility

At the time of writing, the relative perturbation of the solar flux F_D due to non-radial oscillations can be written as:

$$F_D = \frac{F_I^{lm} + F_G^{lm}}{F_0} \tag{11}$$

where F_0 is the unperturbed flux, F_I^{lm} is the perturbation induced by changes in the equilibrium state of the photosphere, both changes of size and of thermodynamic quantities (temperature density, etc...); and F_G^{lm} is the perturbation induces by changes of the surface shape (distortion). With:

$$F_0 = \int_D I\,(\mu)\sin^2\theta \cos\,\phi\ \mathrm{d}\theta\,\mathrm{d}\phi \tag{12}$$

where (θ,ϕ) are the spherical coordinates in the observer's frame (x, y, z), where z is the projection of the rotation axis of the Sun onto the plane of the sky and x is the line of sight; $I\,(\mu)$ is the limb-darkening with $\mu = \sin\ \theta \cos\ \phi$; D is the integration domain (LOI pixels for example); and:

$$F_I^{lm} = \int_D \delta I\,(\mu)\ Y_l^m(\theta,\,\phi\,)\ \sin^2\theta \cos\,\phi\ \ \mathrm{d}\theta\,\mathrm{d}\phi \tag{13}$$

where $\delta I(\mu)$ is an equivalent limb-darkening depending on the mode eigenfunction and model of the solar photosphere (Toutain and Gouttebroze, 1993). For practical purposes, we give here below, in a table, the coefficients for $\delta I(\mu)$ using an adiabatic approximation for the eigenfunction. Hence we write:

$$\delta I\,(\mu) = \sum_{i=0}^{n} a_i\,\mu^i \tag{14}$$

where the a_i are given in Table 1 for a set of low-degree g modes; and in addition we also have:

$$F_G^{lm} = \int_D \left(2I - \left[I + \mu \frac{\mathrm{d}I}{\mathrm{d}\mu} \right] \left[\mathrm{cotg}\theta \frac{\partial}{\partial\theta} - \frac{\mathrm{tg}\,\phi}{\sin^2\theta} \frac{\partial}{\partial\phi} \right] \right) Y_l^m(\theta, \phi) \sin^2\theta \cos\phi \;\mathrm{d}\theta\,\mathrm{d}\phi \qquad (15)$$

Equations (13) and (15) are correct when the pulsation axis z' is also the z axis of the observer's frame. During the SOHO mission this will certainly not be the case. A small correction will be necessary due to the B angle, the P angle will be kept by the spacecraft as close to zero as possible. Therefore, the new F_I^{lm} or F_G^{lm} will be written as:

$$F_{I,G}^{lm} = \sum_{m'=-l}^{m=l} F_{I,G}^{lm}\, d_{m'm}^{(l)}\,(B) \qquad (16)$$

where the rotation matrices $d^{(l)}\,(B)$ can be computed from Edmonds (1957) (See also Appourchaux and Andersen, 1990, for further details). In a first approximation, the B angle will be derived from the ephemeris. A small correction due to the position of the satellite on the halo orbit will be implemented, if necessary.

order	a_0	a_1	a_2
21	0.8544	-32.3683	106.0366
20	0.7589	-28.7309	94.6659
19	0.6698	-25.3014	83.9535
18	0.5840	-22.0435	73.7927
17	0.5039	-18.9810	64.2439
16	0.4279	-16.0947	55.2769
15	0.3565	-13.3725	46.8247
14	0.2896	-10.8102	38.9027
13	0.2259	-8.3727	31.3994
12	0.1645	-6.0507	24.2933
11	0.1078	-3.8646	17.6563
10	0.0535	-1.7864	11.4124
9	0.0013	0.2125	5.5080
8	0.0487	2.1407	-0.0668
7	0.0979	4.0498	-5.4223
6	0.1481	5.9931	10.6591

Table 1: "Limb darkening coefficients" for the lagrangian perturbation of a set of l=2 g modes.

Two different ways of computing F_D have been considered, one using a Lagrangian formulation, the other an Eulerian one (Berthomieu et al 1990, Provost et al 1991, Gouttebroze et al 1994). A comparison of the two methods is being carried on. It shows an agreement between the two results. It appears that the contributions to the flux of the perturbations of source function and of the opacity of the medium almost cancel and that the contribution of the geometrical effects is not negligible. However the effect of convection is not taken into account and this should be one aim of future work.

5.3 Excitation

Several proposal have been made concerning the possible excitation of internal *g* modes. Different types of hydrodynamical instabilities have been proposed, but no definite conclusions have been made. Another possibility is excitation by convective overshoot into the stable interior. Press (1981) has indicated that a feasible mechanism was that the excitation may be driven by the pressure perturbations. Andersen (1994) has studied the excitation numerically by hydrodynamic simulations and find that the overshoot excites gravity waves in the interior with an efficiency equivalent to about 0.1% of the average kinetic energy density in the convection zone. This work will be continued and combined with earlier studies (Andreassen et al 1992; on the transmission efficiency of gravity waves through the convection zone) to give an estimate of the surface amplitudes of *g* modes.

5.4 *g* modes and convection

Interaction between oscillation and convection has been considered for radial modes by Gough 1977, Balmforth 1992a,b and it has been applied to *p* modes. It is desirable to extend this kind of theory to nonradial *g* modes.

Simulations and theoretical considerations (Andreassen et al 1992, Christensen-Dalsgaard 1980) indicate that the transmission of *g* modes through the convection zone depends directly on the depth of the convection and on the l values of the modes. In addition specific combinations of l values and the horizontal scales of motion in the convection zone may decrease or increase the transmission of these modes.

6 Interfacing with other Experiments

6.1 GOLF

The interface to GOLF will mainly consist in getting validated velocity data (in the sense of "true" velocities $\frac{\mathrm{d}r}{\mathrm{d}t}$). They will be used mainly for analyzing the visibility differences between velocity and intensity, that is to confirm theoretical calculation for the p-mode region. Moreover, it will be used to study the phase relationship between velocity and intensity. There will be a co-operative effort of the two teams, the details of which have to be defined.

For the g-mode detection the comparison of the amplitudes and possibly the phases between velocity and intensity will be of crucial importance for the unique identification of the g modes. Together with the LOI data this will probably be the only way of detecting the g modes buried in the solar noise.

6.2 MDI

The MDI team has implemented in the software of the instrument an LOI-like average of the velocity, and probably intensity as well. The average is based on the input provided by T.Appourchaux taking into account the size of the detector and the focal length of the telescope (measured to a precision better than 0.05%). The comparison with the LOI should be therefore made easy. Only the wavelength will be different. The data will be used to study the phase difference between intensity and velocity (Ni line). These data can also be used to detect g modes and to remove the effect of active regions.

The 128×128 pixel flux budget data from MDI/SOI will be used for the studies of the influence of the photospheric manifestations of solar activity on the total and spectral irradiance, e.g. the flux budget of spots, faculae and bright network. Together with the magnetograms from MDI/SOI these images will help to better identify effects and causes of the solar irradiance variability.

6.3 SOHO Corona experiments

The VIRGO investigation has the emphasis on the study of low degree p and g modes. Part of this is to investigate the excitation and damping of the individual modes. For the p modes it is believed that the general excitation is caused by turbulent motion in or near the solar photosphere. Motion in connection with the granular scale convection is a prime candidate. In addition single high energy inputs like solar flares may excite individual modes or re-excite already existing modes through a constructive interference. This process is probably not very important due to limitation in the available energy, however it is needed for an overall understanding of the excitation process and to enable us to single out non-typical mode amplitudes.

On the more exotic side a catalog of cometary impacts may also be useful.

In addition it may be necessary to understand the properties of the "chromospheric" cavity. This may be important in the study of possible resonances between internal gravity modes and atmospheric gravity waves.

In summary the VIRGO would like to have the following inputs from the corona instruments:

- Time, position and energies of flares.
- Images of the sun taken at wavelengths depicting the temperature minimum and transition regions.
- Properties of sun-grazing comets.

These inputs with information about specific events are required within 3
months of the event.

6.4 Ground Based experiments

BISON

Tenerife Helioseismology group "belongs" and "not belongs" to BISON Network, it depends of the point of view. Belongs in the sense that one station is held in Tenerife Observatory from 1975. This station have produced the more continuous and best data of low degree oscillations. We are free to used this data of Tenerife station under our own responsibility, in this sense, the interface with VIRGO is absolutely clear, we will cooperate as it be necessary. Not Belongs in the sense of Network. The data of BISON Network are not shared with the institutes which take part on it, so we can not access to the data of the other BISON stations, in this sense we can not do anything. If sharing of data or other kind of cooperation are requested by VIRGO team, it is necessary to contact the Birmingham BISON headquarters. The velocity data of the

Tenerife station or of the BISON network (if available) will be used to study the phase difference between intensity and velocity (K line).

GONG

So far no formal contact has been taken with the GONG team but since almost any VIRGO CoI should be a GONG member, we should not have any problem to use these data. A formal request may need to be send to the GONG project in due time. The GONG data will be used to study the phase difference between intensity and velocity (Ni line).

IRIS

The relation with IRIS Network is absolutely different, the data of all the stations are shared and no big problems exist. IAC as member of IRIS Network will try to make this interfacing, friendly and improve the VIRGO cooperation. The IRIS data will be used to study the phase difference between intensity and velocity (Na line).

Taiwan Oscillation Network (TON)

TON have now three stations running , Tenerife, Beijing (China) and Big Bear. All instruments works nicely and the quality of images are very high. Other stations will be held soon. The first analysis are now being performed with very nice results. Taking into account the resolution of TON (1100 × 1100 pixels). TON will be a perfect complement to GONG and MDI because none of them have that resolution. Concerning the interfacing with TON Headquarters (Dr Dean Yi Chou, Taiwan) it will be no problem. The TON project is absolutely open to cooperate with other solar experiments. Data to be used are to be defined.

Tenerife LOI

The instrument should be still operational when SOHO flies. If the launch is delayed by 6 months or more, we plan to put a second LOI in Baja, California, Mexico.

7 References

Andersen, B.N., 1994, *Sol. Phys.*, **152**, 241

Andersen, B.N. and Domingo, V., 1988, in *Advances in Helio- and Asteroseismology*, IAU Symposium 123, J,Christensen-Dalsgaard and S.Frandsen eds, Reidel, p. 67

Andersen, B.N., Leifsen, T., Toutain, T., 1994, *Sol. Phys.*, **152**, 247

Andreassen, O., Andersen, B.N. and Wassberg, C.E., 1992, *AA*, **257**, 763

Appourchaux, T. and Andersen, B.N., 1990, *Sol. Phys.*, **128**, 91

Appourchaux, T., Toutain, T., Telljohann, U., Jiménez, A., Rabello-Soares, M.C., Andersen, B.N. and Jones, A.R., 1995, *AA*, **294**, L13

Bachmann, K.T. and Brown, T.M., 1993, *Ap. J. Lett.*, **411**, L45

Balmforth, N.J., 1992a, *MNRAS*, **255**, 603

Balmforth, N.J., 1992b, *MNRAS*, **255**, 639

Berthomieu, G., Gonczi, G., Graff, Ph., Provost, J. and Rocca, A., 1978, *AA*, **70**, 579

Berthomieu, G. and Provost, J., 1990, *AA*, **227**, 563

Chapman, G., 1987, *Ann. Revs. AA.*, **22**, 593.

Christensen-Dalsgaard, J., 1980, *MNRAS*, **190**, 765

Crommelynck, D., Domingo, V., Fichot, A., Fröhlich, C., Penelle, B., Romero J. and Wehrli, Ch., 1993, *Metrologia*, **30**, 375

Edmonds, E.D., 1957, *Angular Momentum in Quantum Mechanics*, 2nd edition, Oxford University Press, Oxford

Foukal, P. and Lean, J., 1988, *Ap. J.*., **328**, 347

Fröhlich, C.: 1990, in *Climate Impact of Solar Variability* , K.H. Schatten and A. Arking eds, NASA Conf. Pub. CP-3086, p. 269.

Fröhlich, C., 1994, in *The Sun as a Variable Star: Solar and Stellar Irradiance Variations*, J.M. Pap, C. Fröhlich, H.S. Hudson and S.K. Solanki eds, Cambridge University Press, Cambridge, p. 217

Fröhlich, C. and Delache, Ph., 1984, in *Solar Seismology from Space*, R.K. Ulrich, J.Harvey, E.J. Rhodes and J.Toomre eds, JPL Publ.84-84, Pasadena, p. 183

Fröhlich, C., Foukal, P., Hickey, J.R., Hudson, H.S. and Willson, R.C., 1990, in *Sun in Time* , C.P. Sonnett, M.S. Giampapa and M.S. Matthews eds, Univ. Arizona Press, p. 11.

Fröhlich, C. and Pap, J., 1989, *AA*, **220**, 272

Fröhlich, C., Toutain, T., Bonnet, R.M., Bruns, A.V., Delaboudinière, J.P., Domingo, V., Kotov, V.A., Kollath, Z., Rashkovsky, D.N., Vial, J.C. and Wehrli, Ch.,

1990, in *Inside the Sun*, Kluwer, G.Berthomieu and M.Cribier eds, Dordrecht, p. 279.
Gough, D.O., 1977, *ApJ*, **214**, 196
Gough, D.O. and Kosovichev, A.G., 1993, *MNRAS*, **264**
Harvey, K.: 1994, in *The Sun as a Variable Star: Solar and Stellar Irradiance Variations* , J.M. Pap, C. Fröhlich, H.S. Hudson and S.K. Solanki eds, Cambridge Univ. Press., p. 217.
Hudson, H.S., 1988, *Ann. Rev. AA*, **26**, 473
Kuhn, J. R: 1994, in *The Sun as a Variable Star: Solar and Stellar Irradiance Variations* , J.M. Pap, C. Fröhlich, H.S. Hudson and S.K. Solanki eds, Cambridge Univ. Press., p. 130.
Kuhn, J.R., Libbrecht, K.G. and Dicke, R., 1988, *Science* , **242**, 908.
Kuhn, J.R. and Libbrecht, K.G., 1991, *ApJ. Lett.*, **381**, L35
Lean, J., 1991, *Rev. Geophys.*, **29**, 505.
Pap, J., Willson, R.C., Fröhlich, C., Donnelly, R.F. and Puga, L., 1994, *Sol. Phys.*, **152**, 13
Press, W.H., 1981, *Ap.J.*, **245**, 286
Provost, J. and Berthomieu, G., 1986, *AA*, **165**, 218
Toutain, T. and Fröhlich, C., 1992, *AA*, **257**, 287
Toutain, T. and Gouttebroze, P., 1993, *AA*, **268**, 309
Gouttebroze, P. and Toutain, T., 1994, *AA* , **287**, 535
Provost, J. and Berthomieu, G., 1991, *Adv. Space Res.*, **11**, 4, 39
Romero, J., Wehrli, C. and Fröhlich, C., 1994, *Sol. Phys.*, **152**, 23
Willson, R.C., 1992, *EOS Transactions*, AGU, **73 (14)**, 242
Willson, R.C., Gulkis, S., Janssen, M., Hudson, H.S. and Chapman, G., 1981, *Science*, **211**, 700.
Willson, R.C. and Hudson, H.S., 1988a, *Nature*, **332**, 332
Willson, R.C. and Hudson, H.S., 1988b, *Nature*, **332**, 810
Willson, R.C. and Hudson, H.S., 1991, *Nature*, **351**, 42
Woodard, M. and Hudson, H.S., 1983, *Sol. Phys.*, **82**, 67.
Wolff, C., 1984, *Sol.Phys.*, **93**, 1